Hindawi Publishing Corporation
International Journal of Antennas and Propagation
Volume 2013, Article ID 571975, 8 pages
http://dx.doi.org/10.1155/2013/571975

Research Article

Broadband EM Performance Characteristics of Single Square Loop FSS Embedded Monolithic Radome

Raveendranath U. Nair, J. Madhumitha, and Rakesh M. Jha

Computational Electromagnetics Laboratory, Centre for Electromagnetics, CSIR-National Aerospace Laboratories (CSIR-NAL), Bangalore 560017, India

Correspondence should be addressed to Raveendranath U. Nair; raviunair@nal.res.in

Received 15 June 2012; Revised 11 February 2013; Accepted 18 February 2013

Academic Editor: Stefano Selleri

A monolithic half-wave radome panel, centrally loaded with aperture-type single square loop frequency selective surface (SSL-FSS), is proposed here for broadband airborne radome applications. Equivalent transmission line method in conjunction with equivalent circuit model (ECM) is used for modeling the SSL-FSS embedded monolithic half-wave radome panel and evaluating radome performance parameters. The design parameters of the SSL-FSS are optimized at different angles of incidence such that the new radome wall configuration offers superior EM performance from L-band to X-band as compared to the conventional monolithic half-wave slab of identical material and thickness. The superior EM performance of SSL-FSS embedded monolithic radome wall makes it suitable for the design of normal incidence and streamlined airborne radomes.

1. Introduction

Enhancement of radome performance parameters over broadband is a major challenge in the design of airborne radomes for modern radar antenna systems. Over broadband of frequencies, major goals to achieve are high transmission efficiency, low cross-polar levels, and low boresight error characteristics with possible modifications of radome wall configurations. Many techniques were reported for modifying the radome wall configurations to enhance the EM performance of radome walls [1, 2]. Generally, arrays of thin parallel metallic wires and wire meshes were used for the broadbanding of radomes. The application of single-wire grid and double-wire grid was proposed for the broadbanding of thin dielectric slabs [3]. The EM performance of modified A-sandwich panels by matching core to that of the skin was studied by Chase [4]. Monolithic radome panels, centrally loaded by a periodic array of conducting inclusions, offered a wider frequency bandwidth compared to the conventional radome designs of the same material and thickness [5, 6]. In some other applications, resonant walls made of perforated metal sheet structures were embedded within the dielectric wall or fixed behind the dielectric radome panel. Such structures had narrow bandwidth but provided better performance at the high-incidence angles.

Most of the reported works focused on the enhancement of transmission efficiency of the radome panels. Even though the transmission efficiency of the radome wall configurations can be improved with the inclusion of metallic structures, other performance parameters like boresight error, cross-polar level, and so forth, may degrade drastically. This necessitates the development of new techniques, which can simultaneously improve the EM performance parameters of radome walls. In this regard, FSSs find potential applications in the design of high-performance radomes due to their inherent frequency selective characteristics [7]. In our previous work reported elsewhere [8], circular FSS was used for the enhancement of EM performance parameters of monolithic half-wave radome over X-band. For the equivalent transmission line model of circular FSS embedded radome wall structure, the circular FSS was considered as an inductive element and hence the inductive susceptance of circular FSS was incorporated in the EM analysis. This representation may not be valid for all the frequencies considered in the X-band.

In the present work, novel application of aperture type single square loop (SSL) frequency selective surface for

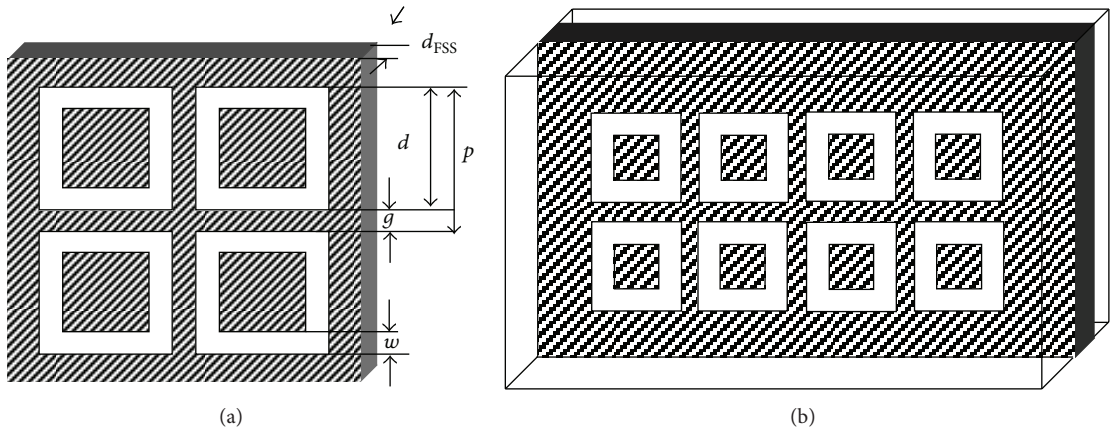

Figure 1: (a) Schematic of the single square loop (SSL)-FSS and (b) Monolithic slab of half-wave thickness. SSL-FSS is centrally loaded *w.r.t.* the midplane. Here p: periodicity; d_{FSS}: thickness of SSL-FSS; g: gap length; d: length of SSL element; and w: width of SSL element.

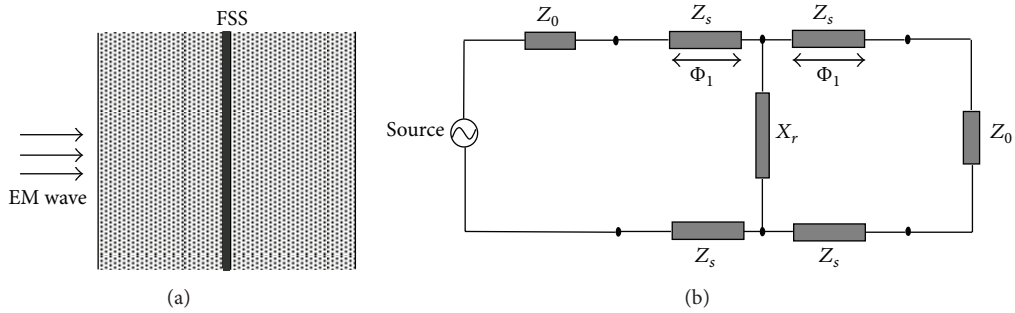

Figure 2: (a) Schematic of the monolithic half-wave slab centrally loaded with SSL-FSS and (b) its equivalent circuit.

broadbanding of monolithic half-wave radome wall configuration is presented (Figure 1). Here the reactance (which consists of both inductive and capacitive components) of the SSL-FSS element is included in the EM performance analysis of SSL-FSS embedded radome wall. Hence, it offers a better representation of the SSL-FSS element in the equivalent transmission line model of the cascaded radome wall configuration (Figure 2).

Monolithic half-wave radome wall is generally used for the design of streamlined nose-cone radomes as it provides superior EM performance at the design frequency and sufficient structural rigidity for catering extreme aerodynamic stresses at high Mach speeds. But the major disadvantage of monolithic half-wave wall is very narrow bandwidth, which limits its applications. Since modern airborne radar antennas have multiband functional requirements, such designs may not be sufficient. Hence, in the present work, the design parameters of SSL-FSS embedded monolithic half-wave wall configuration are optimized such that they provide superior EM performance as compared to monolithic radome panel alone over the entire frequency range from L-band to X-band and over a range of incidence angles.

It is observed that for a given radome wall configuration with identical materials and dimensions, the radome EM performance characteristics are generally superior for parallel polarization, as compared to perpendicular polarization at a given incidence angle [1]. In other words, the performance degradations for a given radome wall configuration may be more for the perpendicular polarization case as compared to the parallel polarization case. Hence, in the present work, the EM performance parameters for perpendicular polarization are analyzed.

2. EM Modeling Aspects

Monolithic half-wave radome wall considered is made of typical glass epoxy ($\varepsilon_r = 4.0$; $\tan\delta_e = 0.015$). The radome wall thickness (d_m), optimized for power transmission at the midfrequency of X-band and at normal incidence, is 7.44 mm. It is selected based on the fact that the half-wave radome wall thickness at the lower frequency range is very large, thereby making the radome panel heavy and conflicting with the weight requirements. The single square loop FSS, consisting of periodic arrays of square loop apertures, is centrally loaded in the monolithic half-wave radome wall.

The SSL-FSS embedded monolithic radome wall is considered as an equivalent transmission line with different sections corresponding to slab and FSS structure (Figure 2). The change in the characteristic impedance of the free space and monolithic half-wave wall is a major source of reflection of the wave incident on the structure. In the present radome

wall structure, SSL is symmetrically loaded in the midplane of the monolithic slab.

As compared to the free space, different layers of SSL-FSS embedded monolithic wall can be considered as low impedance lines connected end to end. Hence, the whole configuration can be represented by a single matrix obtained by the multiplication of matrices corresponding to the individual layers.

Since the SSL-FSS is located in the midplane of the monolithic slab, it is considered to be made up of two identical sections with SSL-FSS in between them. Let Z_0 be the characteristic impedance of free space. The characteristic impedance of each half-section of monolithic slab is represented by Z_s. In the equivalent transmission line method, the matrix consisting of A_i, B_i, C_i, and D_i will represent the ith layer of the radome wall. Let t and d_{FSS} represent the thickness of each half-section of monolithic slab and SSL-FSS, respectively. Here, $t = (d_{\text{m}} - d_{\text{FSS}})/2$.

One half-section of the wall is represented by

$$\begin{bmatrix} A_1 & B_1 \\ C_1 & D_1 \end{bmatrix} = \begin{bmatrix} \cos\,\Phi_1 & j\dfrac{Z_s}{Z_0}\sin\,\Phi_1 \\ j\dfrac{Z_0}{Z_s}\sin\,\Phi_1 & \cos\,\Phi_1 \end{bmatrix}, \tag{1}$$

where Φ is the electrical length corresponding to each layer, which is a function of the complex permittivity, ε^*, of dielectric layer, the angle of incidence, θ, and the thickness of the dielectric layer, d. The other half-section of the wall is represented by

$$\begin{bmatrix} A_2 & B_2 \\ C_2 & D_2 \end{bmatrix} = \begin{bmatrix} \cos\Phi_2 & j\dfrac{Z_s}{Z_0}\sin\Phi_2 \\ j\dfrac{Z_0}{Z_s}\sin\Phi_2 & \cos\,\Phi_2 \end{bmatrix}. \tag{2}$$

The interaction of incident EM waves with aperture type FSS is represented as a wave propagating along a transmission line, with shunt reactance representing the FSS. The EM characteristics of single unit cell of SSL-FSS are assumed to be same as that of infinite periodic array. The monolithic half-wave slab exhibits a capacitive reactance, while the aperture type SSL-FSS exhibits inductive reactance. The design parameters of the aperture type SSL-FSS are optimized in such a way that the inductive reactance of SSL-FSS matches the capacitive reactance of the entire monolithic slab to provide broadband EM performance. Let A_{FSS}, B_{FSS}, C_{FSS}, and D_{FSS} be the elements of the matrix representing aperture type SSL-FSS. Then, the SSL-FSS is represented by the following:

$$\begin{bmatrix} A_{\text{FSS}} & B_{\text{FSS}} \\ C_{\text{FSS}} & D_{\text{FSS}} \end{bmatrix} = \begin{bmatrix} 1 & 0 \\ \dfrac{1}{jX_r} & 1 \end{bmatrix}. \tag{3}$$

Here, X_r represents the reactance of the SSL-FSS, which is a function of inductive reactance X and capacitive susceptance B. The equivalent circuit modeling of SSL-FSS was discussed in [9]. Using this modeling approach, X and B are given by

$$X = \frac{p\cos\theta}{\lambda}\left[\ln\left(\frac{1}{\sin\left(\pi w/2p\right)}\right)\right],$$
$$B = \frac{4p\sec\theta}{\lambda}\left[\ln\left(\frac{1}{\sin\left(\pi g/2p\right)}\right)\right]. \tag{4}$$

Here, w, g, and p are the width, gap width, and period of the SSL-FSS, respectively. λ is the wavelength of the incident EM wave. In order to eliminate spurious reflections and phase distortions, the medium present in the aperture sections of the SSL-FSS is assumed to be the same as that of the monolithic radome wall. The entire monolithic half-wave wall with SSL-FSS is represented by [10] as follows:

$$\begin{bmatrix} A & B \\ C & D \end{bmatrix} = \begin{bmatrix} A_1 & B_1 \\ C_1 & D_1 \end{bmatrix}\begin{bmatrix} 1 & 0 \\ \dfrac{1}{jX_r} & 1 \end{bmatrix}\begin{bmatrix} A_2 & B_2 \\ C_2 & D_2 \end{bmatrix}. \tag{5}$$

Using (3), the A, B, C, and D parameters of the final matrix are computed. The power transmission coefficient is given by the following:

$$p_{tr} = \left[\frac{4}{(A+B+C+D)^2}\right]. \tag{6}$$

The power reflection coefficient is given by the following:

$$p_{rf} = \left[\frac{A+B-C-D}{A+B+C+D}\right]^2. \tag{7}$$

The phase distortions are determined by the insertion phase delay (IPD) of the radome wall. For the present radome wall configuration, two symmetric dielectric layers and one FSS layer are cascaded. Hence, the insertion phase delay is given by the following:

$$\text{IPD} = -\angle T - \frac{2\pi}{\lambda}\left(2t + d_{\text{FSS}}\right)\cos\,\theta. \tag{8}$$

Table 1 shows the optimized design parameters of the SSL-FSS over 1 GHz–12 GHz at normal incidence, 30°, 45°, and 60°. Here, width w and d_{FSS} are kept constant from the fabrication point of view. Other design parameters (d, g, and p) are optimized in such a way that the resulting FSS-based radome wall configuration would provide maximum power transmission and minimum power reflection and insertion phase delay over the specified frequency range.

Table 1: Design parameters of SSL-FSS.

Angle of incidence	Length, d (mm)	Width, w (mm)	Gap length, g (mm)	Period, p (mm)	Thickness, d_{FSS} (mm)
0°	13.20	3.0	2.0	15.20	3.0
30°	10.25	3.0	1.0	11.25	3.0
45°	12.00	3.0	1.0	13.00	3.0
60°	17.00	3.0	1.0	18.00	3.0

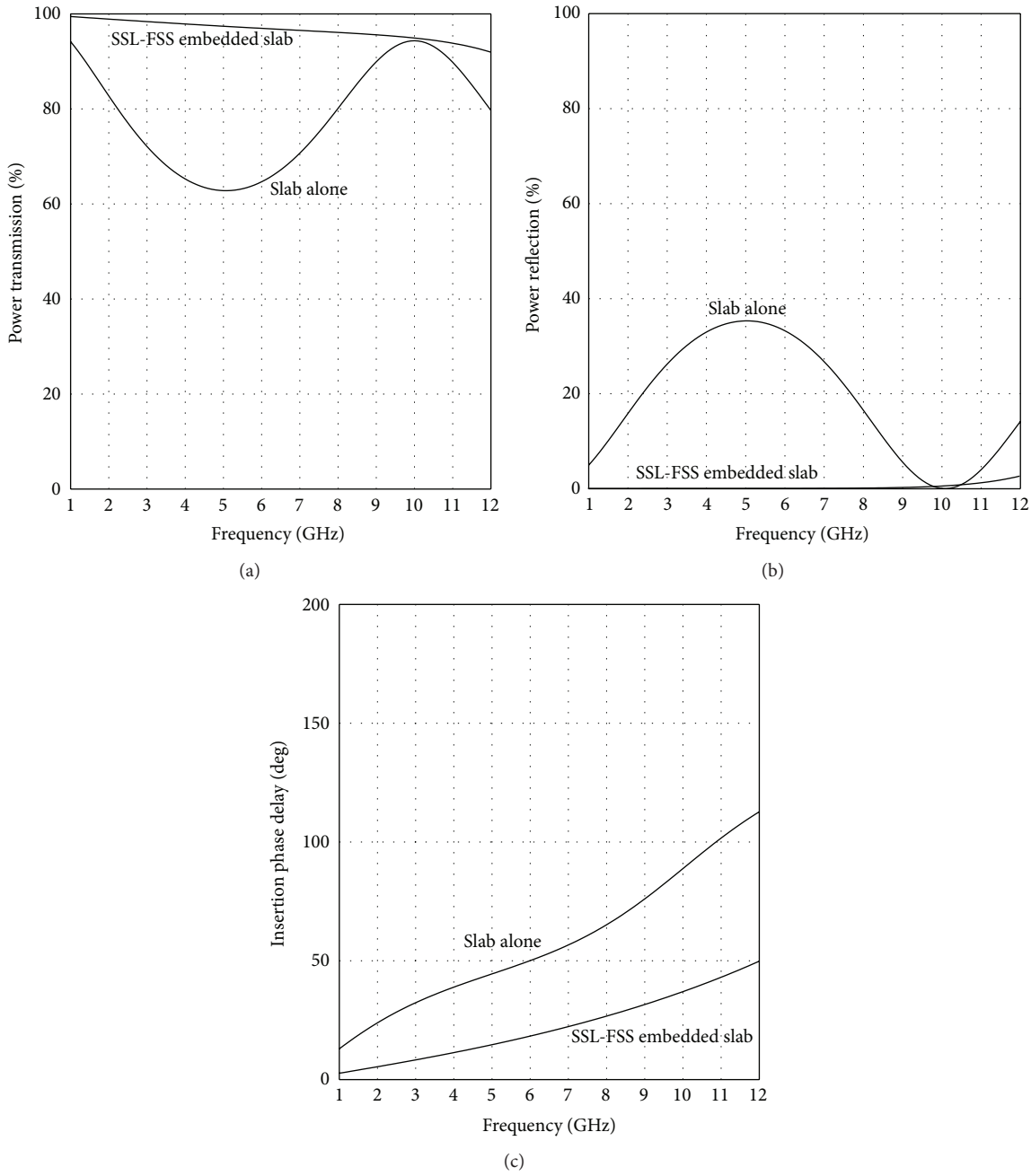

Figure 3: (a) *SSL-FSS embedded monolithic half-wave slab design* results in higher power transmission characteristics at normal incidence over a broadband (1 GHz–12 GHz) as compared to the *slab alone* case. (b) *SSL-FSS embedded monolithic half-wave slab design* results in lower power reflection characteristics at normal incidence over a broadband (1 GHz–12 GHz) as compared to the *slab alone* case. (c) *SSL-FSS embedded monolithic half-wave slab design* results in superior insertion phase delay characteristics at normal incidence over a broadband (1 GHz–12 GHz) as compared to the *slab alone* case.

3. Numerical Results and Discussion

Here, $\angle T$ is phase angle associated with the voltage transmission coefficient of the entire radome wall. It is noted that the length, d, and gap width, g, of SSL-FSS are critical design parameters and any slight variations in these dimensions alter the EM performance parameters drastically.

The EM performance parameters (power transmission, power reflection, and insertion phase delay) of the monolithic configuration with SSL-FSS are computed for perpendicular polarization over a range of incidence angles (0°, 30°, 45°, and 60°). The incidence angles in the range 0°–30° are typical for normal incidence radomes (hemispherical and cylindrical shapes), 0°–45° for paraboloidal radomes, and 0°–60°

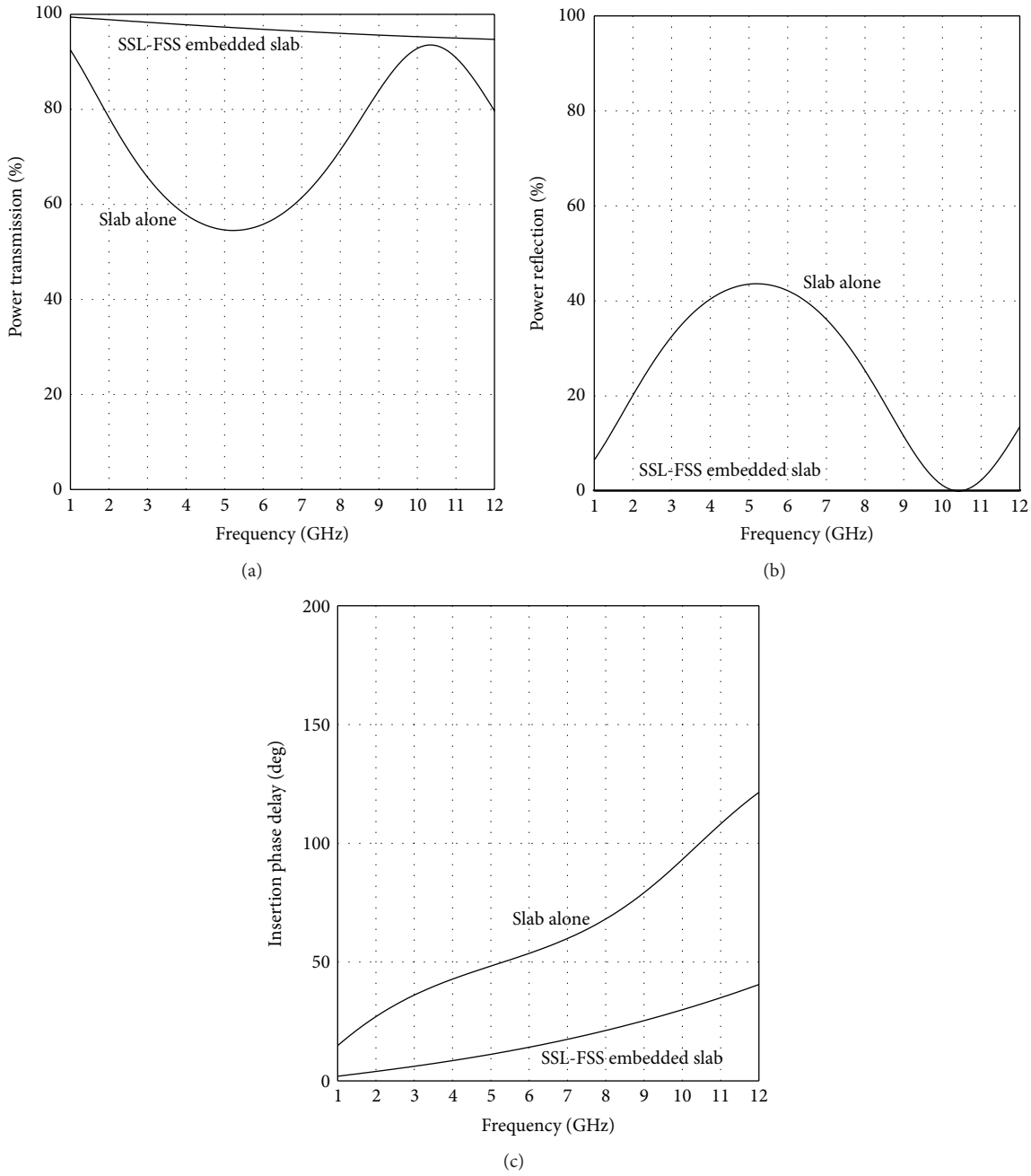

Figure 4: (a) *SSL-FSS embedded monolithic half-wave slab design* results in higher power transmission characteristics at 30° over a broadband (1 GHz–12 GHz) as compared to the *slab alone* case. (b) *SSL-FSS embedded monolithic half-wave slab design* results in lower power reflection characteristics at 30° over a broadband (1 GHz–12 GHz) as compared to the *slab alone* case. (c) *SSL-FSS embedded monolithic half-wave slab design* results in superior insertion phase delay characteristics at 30° over a broadband (1 GHz–12 GHz) as compared to the *slab alone* case.

for the highly streamlined radomes (conical, ogival radome, etc.). A comparative study of the EM performance of SSL-FSS monolithic half-wave radome with that of monolithic slab alone is presented in the following sections.

3.1. EM Performance at Normal Incidence. The power transmission characteristics of the monolithic slab alone and SSL-FSS embedded monolithic slab over the frequency range 1 GHz–12 GHz at normal are shown in Figure 3(a). The power transmission characteristic of monolithic slab alone, at normal incidence is high, around 95% at 1 GHz, and decreases gradually to the minimum around 5 GHz. Thereafter, the power transmission efficiency gradually increases to a high value at the design frequency (10 GHz) of the monolithic slab. With the incorporation of SSL-FSS, the transmission efficiency of the monolithic half-wave panel has been improved considerably throughout the frequency range,

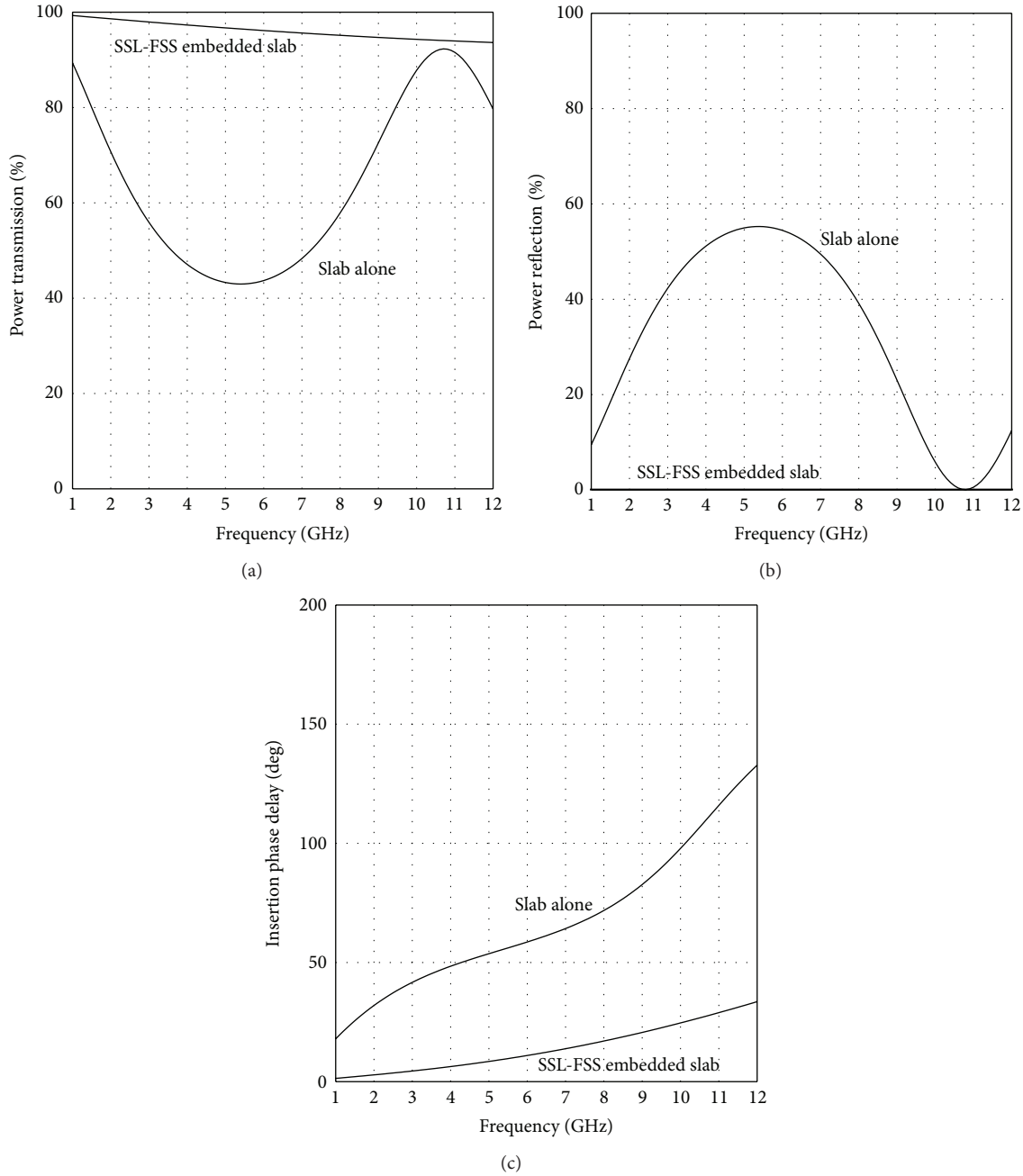

Figure 5: (a) *SSL-FSS embedded monolithic half-wave slab design* results in higher power transmission characteristics at 45° over a broadband (1 GHz–12 GHz) as compared to the *slab alone* case. (b) *SSL-FSS embedded monolithic half-wave slab design* results in lower power reflection characteristics at 45° over a broadband (1 GHz–12 GHz) as compared to the *slab alone* case. (c) *SSL-FSS embedded monolithic half-wave slab design* results in superior insertion phase delay characteristics at 45° over a broadband (1 GHz–12 GHz) as compared to the *slab alone* case.

and it is superior to those for the slab alone case. However, the transmission efficiency of SSL-FSS embedded structure shows gradual decrease from 1 GHz to 12 GHz.

The power reflection is almost negligible in the frequency range from 1 GHz to 10 GHz and it shows slight increase beyond 10 GHz (Figure 3(b)). For monolithic slab alone, the power reflection characteristic demonstrates oscillatory nature. It starts increasing from 1 GHz, reaches maximum (around 35%) at 5 GHz, followed by decrease to a very low value at the design frequency of 10 GHz, and increases thereafter. It is interesting to note that the power reflection of SSL-FSS embedded structure is very low (well within 5%) throughout the frequency range.

3.2. EM Performance at 30°. The EM performance characteristics of the SSL-FSS embedded and slab alone structures at the incidence angle 30° are shown in Figures 4(a)–4(c). Similar to the normal incidence, the power transmission

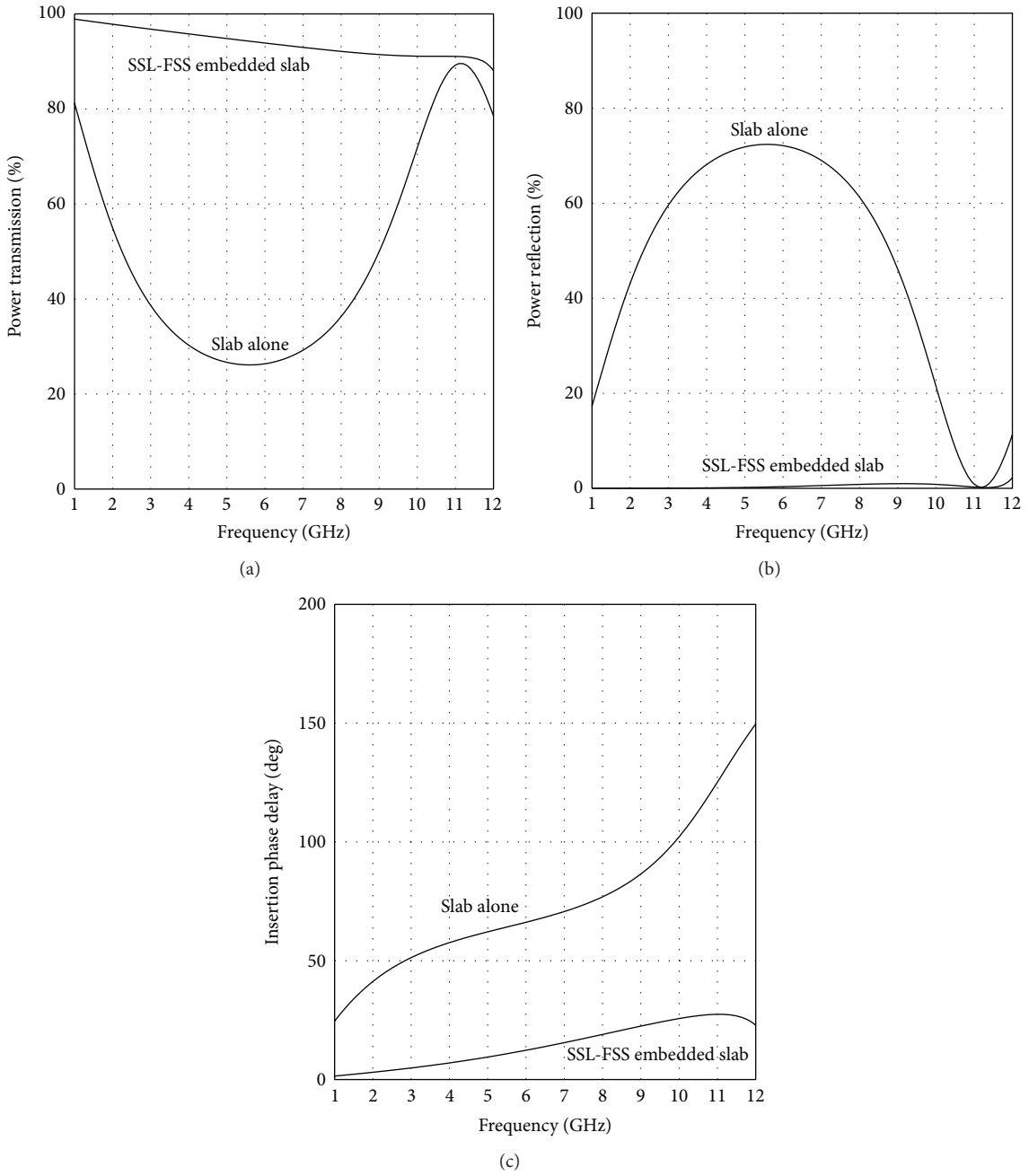

Figure 6: (a) *SSL-FSS embedded monolithic half-wave slab design* results in higher power transmission characteristics at 60° over a broadband (1 GHz–12 GHz) as compared to the *slab alone* case. (b) *SSL-FSS embedded monolithic half-wave slab design* results in lower power reflection characteristics at 60° over a broadband (1 GHz–12 GHz) as compared to the *slab alone* case. (c) *SSL-FSS embedded monolithic half-wave slab design* results in superior insertion phase delay characteristics at 60° over a broadband (1 GHz–12 GHz) as compared to the *slab alone* case.

efficiency of SSL-FSS embedded panel is much better than that of slab alone. As compared to the normal incidence case, the power transmission efficiency of SSL-FSS has been improved.

The power reflection of SSL-FSS embedded panel is almost zero throughout the entire frequency range, which is highly desirable for radome applications. This is in contrast to the slab alone case for which the power reflection characteristic is oscillatory. Very low reflection is essential for reducing the sidelobe level degradation and elimination of flash lobes. As in the case of normal incidence, the IPD of SSL-FSS embedded panel is lower than that of monolithic slab alone structure. But the IPD of SSL-FSS embedded panel has been reduced as compared to that of normal incidence case.

3.3. EM Performance at 45°. The power transmission, power reflection, and IPD characteristics of SSL-FSS embedded

monolithic slab and slab alone at 45° are shown in Figures 5(a)–5(c), respectively. Similar to the previous cases, the power transmission of SSL-FSS embedded wall is much better than that of slab alone throughout the frequency range. The power reflection for the modified structure is also very low (close to zero) in the entire frequency range. Regarding insertion phase delay, the SSL-FSS embedded wall shows better performance as compared to the slab alone.

3.4. EM Performance at 60°. The EM performance characteristics of both SSL-FSS embedded and slab alone structures at high incidence angle 60° are shown in Figures 6(a)–6(c). As compared to the previous incidence angle cases, there is a decrease in the power transmission efficiency of SSL-FSS embedded radome panel. Even though the power reflection of SSL-FSS embedded wall is very low as compared to that of slab alone case, it has increased in the high-frequency region.

The IPD of SSL-FSS embedded wall is also lower than that of slab alone. It is observed that the IPD of SSL-FSS embedded structure tends to fall in the higher frequency end. These results indicate that the SSL-FSS embedded monolithic half-wave wall will offer better boresight error (BSE) characteristics (which is an associated parameter of IPD), as compared to monolithic radome case alone.

4. Conclusions

The EM analysis shows that this novel application of SSL-FSS radome design is capable of achieving broadbanding of monolithic half-wave radome panels over a wide range of incidence angles such as those found in advanced aerospace/aircraft applications. Thus this radome structure has overcome the major limitation of the conventional monolithic half-wave radome wall, that is, the very narrow bandwidth. Considering the EM performance parameters, the SSL-FSS is found to be a better choice as compared to circular FSS [8] for radome broadbanding application. Moreover, the presence of FSS in the radome wall offers more structural rigidity, which an advantage for the airborne applications. The present work also shows that the SSL-FSS embedded monolithic half-wave radome wall configuration has potential application in the design of both the normal-incidence radomes and the highly streamlined nose-cone radomes.

References

[1] R. H. J. Cary, "Radomes," in *The Handbook of Antenna Design*, A. W. Rudge, K. Milne, A. D. Olver, and P. Knight, Eds., Peter Peregrinus, London, UK, 1982.

[2] D. J. Kozakoff, *Analysis of Radome Enclosed Antennas*, Artech House, Norwood, Mass, USA, 2009.

[3] M. A. Teichman, "Designing wire grids for impedance matching of dielectric sheets," *Microwave Journal*, vol. 11, pp. 73–78, 1968.

[4] V. A. Chase, "Investigation of improved composites for radome applications," in *Proceedings of 13th Symposium on Electromagnetic Windows*, pp. 23–28, Georgia Institute of Technology, 1976.

[5] A. Frenkel, "On the scaling of inclusions size in metal-dielectric windows at normal incidence," *IEEE Antennas and Wireless Propagation Letters*, vol. 1, pp. 26–27, 2002.

[6] A. Frenkel, "Thick metal-dielectric window," *Electronics Letters*, vol. 37, no. 23, pp. 1374–1375, 2001.

[7] B. A. Munk, *Frequency Selective Surfaces: Theory and Design*, Wiley, New York, NY, USA, 2000.

[8] R. U. Nair, T. Madhulatha, and R. M. Jha, "Novel application of circular frequency selective surface for broadbanding of monolithic radome," in *Proceedings of the 7th International Symposium on Management, Engineering and Informatics (MEI '11)*, vol. II, pp. 40–44, Orlando, Fla, USA, 2011.

[9] M. Ohira, H. Deguchi, M. Tsuji, and H. Shigesawa, "Analysis of frequency selective surface with arbitrarily shaped element by equivalent circuit model," *Electronics and Communications in Japan*, vol. 88, no. 6, pp. 9–17, 2005.

[10] F. Chen, Q. Shen, and L. Zhang, "Electromagnetic optimal design and preparation of broadband ceramic radome material with graded porous structure," *Progress in Electromagnetics Research*, vol. 105, pp. 445–461, 2010.